J. Fluid Mech. (1982), *vol.* 118, *pp.* 109–122
Printed in Great Britain

Motion of air cavities in long horizontal ducts

By D. L. WILKINSON

Water Research Laboratory, University of New South Wales,
Manly Vale, N.S.W., Australia

(Received 2 February 1981)

This paper describes an experimental study of the flow associated with the intrusion of an air cavity into a long horizontal duct as water was allowed to drain from one end. Flows of this nature were discussed by Benjamin (1968), who showed that throttling of the flow of water from the end of the duct would cause both the celerity and the depth of the cavity to reduce. However, the experiments described in this paper revealed that the celerity of the cavity was not reduced from its unthrottled value until the water depth beneath the cavity was 0·78 of the duct depth. For values of this depth ratio between 0·5 and 0·78, the flow as a whole was unsteady. It is shown that Benjamin's model can be modified to allow for the unsteady nature of the flow. Benjamin's original model was found to describe accurately the form and behaviour of the cavity in the case of unthrottled flow, when the flow was steady, and also when the depth beneath the cavity exceeded 0·78 of the duct height, when the flow was again steady. Surface-tension effects were found to reduce the celerity of the cavity and to modify its shape as described by Gardner & Crow (1970).

1. Introduction

This paper describes an experimental study of the motion of an air cavity into a long horizontal duct of rectangular cross-section. The motion is initiated by filling the duct completely with water and then partially opening one end of the duct, allowing water to flow out of the duct and air to enter.

Benjamin (1968) suggested such a study might be performed to test the validity of a model he proposed for the motion of gravity currents confined between horizontal boundaries. The model was idealized in that the fluids were assumed to be immiscible, and that effects due to surface tension and viscosity were assumed negligible compared with those relating to fluid inertia and gravity. Benjamin examined the balance of pressure forces and fluid momentum associated with a control volume which moved with the front of the air cavity, and showed that the velocity of the cavity was influenced by the proximity of the lower boundary. It was shown that before steady parallel flow could be achieved downstream of the cavity some energy dissipation was required, except for one flow state when the air–water interface was located midway between the upper and lower boundaries. In this case uniform flow could be achieved beneath the cavity without any energy being dissipated.

Benjamin used conformal mapping to obtain an approximate expression for the shape of the cavity and also examined the stability of the flow with regard to interfacial disturbances.

The experiments by Zukoski (1966) on the motion of long bubbles in closed tubes

provided verification for Benjamin's analysis of the energy-conserving flow in ducts of circular cross-section.

Later work by Gardner & Crow (1970) investigated the effects of surface tension on the energy-conserving flow and showed that surface tension produced significant departures from the cavity shape and celerity calculated by Benjamin. Surface-tension effects were appreciable at surprisingly large scales and, in ducts 100 mm deep, the velocity of the cavity front was some 10 % less than the value predicted by the idealized model, although it will be shown that other factors contributed to this disparity.

Both Zukoski (1966) and Gardner & Crow (1970) found that viscosity had no effect on the initial velocity of the cavity for flows with Reynolds numbers in excess of about 200. The Reynolds number was based on the depth of the duct and the celerity of the cavity. However, in very long ducts, viscous effects must ultimately exert a controlling influence on the flow.

In the experiments described here, both the energy-conserving flow and the non-conserving flows were studied. This was achieved by throttling the discharge from the duct over a weir located across the open end of the duct. Thus the ratio of the cavity depth to the height of the duct could be controlled independently. Gardner & Crow only examined unthrottled flows, in which case ratio of cavity depth to the height of the duct was found to approach the value of $\frac{1}{2}$ in the larger-scale experiments, as predicted by Benjamin's theory.

Once the flow was throttled, the flow as a whole became unsteady, with the head of the cavity progressing forward at the depth and speed that it would have if the duct were open-ended. Behind the head followed a slower moving bore, which defined the limit of upstream influence of the control weir. As the height of the weir was increased, the flow depth on the downstream side of the bore and the celerity of the bore also increased. Finally, when the downstream depth was equal to 0·78 of the height of the duct, the bore moved with the same speed as the cavity, and the flow became steady.

Benjamin in his original work assumed that steady flow could be achieved at all degrees of throttling. The experiments described in this paper show that this is not the case and that the flow as a whole is unsteady when the flow depth far downstream is between $\frac{1}{2}$ and 0·78 of the height of the duct.

A detailed description of an unsteady air-cavity experiment is given in §2. In §3 Benjamin's model is reworked with allowance made for the unsteady nature of the flow. The experiments and experimental techniques are described in §4, and the effects of surface tension and viscosity on the motion of air cavities are discussed in §5.

2. Description of the unsteady flow

Figure 1 shows sequential photographs from an air-cavity experiment in which the flow of water from the duct was impeded by a sharp-crested weir located at the open end of the duct. The height of the weir in this experiment was one-third of the height of the duct. The water was dyed red, and in the photographs shows up dark beneath the white air cavity above. The upper and lower boundaries of the duct are clearly visible and V-shaped distance markers are located at intervals of 20 cm along the upper boundary.

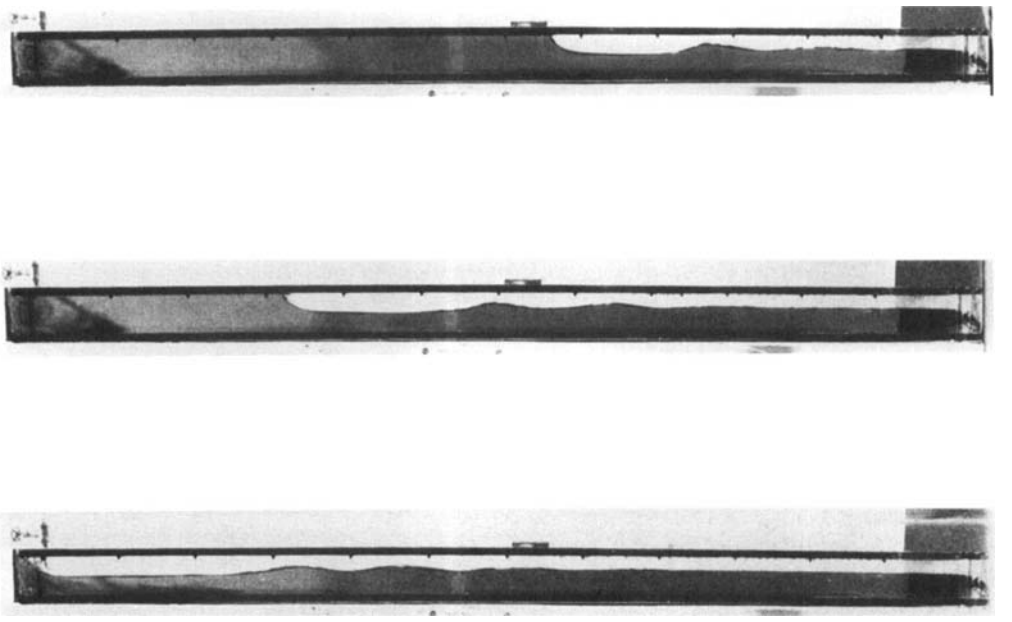

FIGURE 1. Motion of an air cavity in a horizontal duct. Photographs show the cavity at times $t(g/H)^{\frac{1}{2}} = 0{\cdot}24$, $0{\cdot}39$ and $0{\cdot}55$ in the 100 mm high duct. Values of the experimental parameters are $F = 0{\cdot}46$, $F_b = 0{\cdot}32$, $H_1 = 0{\cdot}48$, $H_2 = 0{\cdot}62$ and $\Sigma = 3 \times 10^{-3}$.

The flow can be divided into three distinct regions. At the very front of the air cavity, the elevation of the air–water interface is seen to vary rapidly, but, at a distance of the order of the duct height behind the leading edge, the interface attains a uniform level very nearly at the mid-height of the duct. Here the streamlines are straight and parallel. In the absence of any obstruction at the open end of the duct, this region of uniform flow with the air–water interface at mid-height extended the full length of the cavity. However, the presence of the weir in this experiment caused a bore to propagate upstream behind the head. This bore, which was undular in form, is clearly visible in figure 1 and forms the second flow region. The mean depth can be seen to increase across the bore. Note that there is no evidence of turbulence or energy dissipation in the region ahead of the bore. Finally, a third region can be identified behind the bore, where the free surface is again nearly horizontal, there are no waves, and the flow is uniform.

Having identified the basic features of the flow, it is of interest to follow their development in time as the air cavity progresses along the duct. Examination of the three photographs in figure 1 reveals no variation in the shape of the head with time. However, the frontal region lengthened with time, indicating that the celerity of the cavity front exceeded that of the bore. The undular bore also underwent change as it travelled along the duct. The wave train following the bore front continued to lengthen, thereby providing the mechanism by which energy could be radiated away from the bore. This process is a consequence of the difference in phase speed and group velocity of waves within the train.

Raising the weir caused the depth in the region downstream of the bore to increase, thereby strengthening the bore. This was evidenced by an increase in the amplitudes of the undulations until the leading wave broke and the bore front became turbulent.

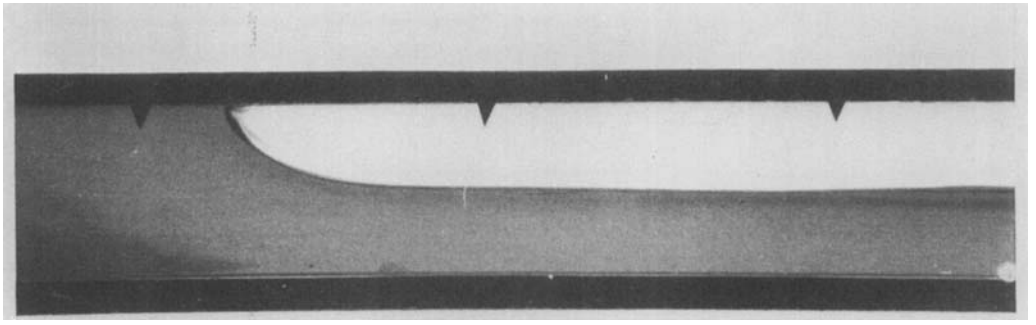

FIGURE 2. Photograph of the energy-conserving flow in the 100 mm high duct. Values of the experimental parameters are $F = 0{\cdot}468$, $H_1 = 0{\cdot}48$ and $\Sigma = 3 \times 10^{-3}$.

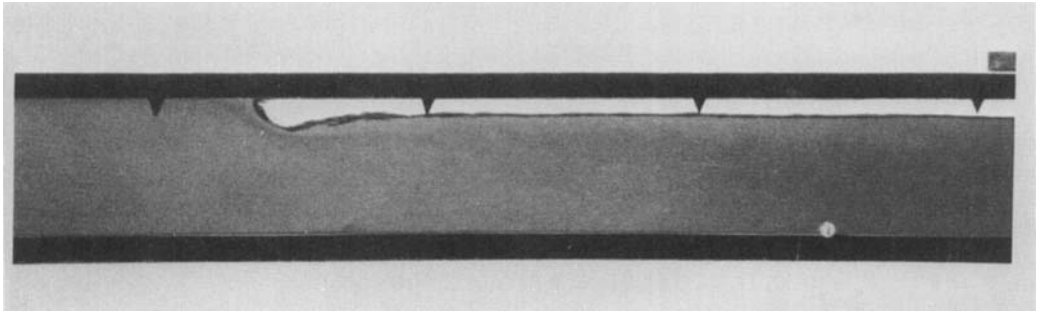

FIGURE 3. Photograph of a flow in which the upstream influence of the control extends to the very front of the cavity. Values of the experimental parameters are $F = 0{\cdot}375$, $H_2 = 0{\cdot}87$ and $\Sigma = 3 \times 10^{-3}$.

Energy that was previously radiated away from the bore by the waves was now dissipated by turbulence within the bore. Once breaking was initiated, the wave amplitudes were much diminished. Increasing the height of the weir also caused the celerity of the bore to increase.

Thus three possible flow regimes were identified and their existence was found to depend on the relative velocities of the cavity front and the bore.

(i) The steady-flow regime in which energy was conserved. This is shown in figure 2, and exists in regions beyond the influence of any downstream control.

(ii) The unsteady regime shown in figure 1, in which an energy-conserving region of continuously increasing length was followed by a bore and developing train of waves.

(iii) The steady dissipative regime which exists when the water depth beneath the cavity exceeds 0·78 of the duct height. This regime is shown in figure 3.

3. Analysis

Although the flow associated with the intrusion of an air cavity into a long duct may be unsteady, selection of suitable frames of reference enables the frontal region, and the bore region to be viewed as steady flows. These two frames of reference, one moving with the cavity front and the other moving with the bore, can be coupled by considering the continuity of the flow beneath the cavity. This enables an analysis to be made of the entire flow field.

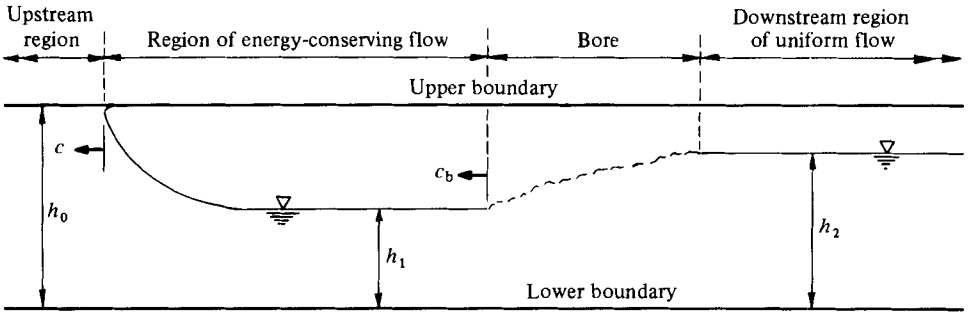

FIGURE 4. Schematic diagram of the flow.

As no energy dissipation is evident upstream of the bore, it is reasonable to assume that energy is conserved in that region. Following Benjamin (1968) and travelling with the front of the air cavity, conservation equations can be written for the fluxes of mass, flow force and energy. With reference to figure 4 these equations are given by

$$\rho c h_0 = \rho u_1 h_1, \tag{1}$$

$$\rho c^2 h_0 + \tfrac{1}{2}\rho g h_0^2 + p_0 h_0 = \rho u_1^2 h_1 + \tfrac{1}{2}\rho g h_1^2 + p_1 h_0, \tag{2}$$

$$\tfrac{1}{2}\rho c^3 h_0 + \rho g c h_0^2 + c h_0 p_0 = \tfrac{1}{2}u_1^3 h_1 + \rho g u_1 h_1^2 + u_1 h_1 p_1, \tag{3}$$

where the subscripts 0 and 1 refer to regions of uniform flow upstream and downstream of the front, and h is the depth of flow, u is the mean velocity relative to axes moving with the front of the cavity, ρ is the density of the lower fluid, and p is the pressure at the upper boundary. The density of the air is assumed negligible compared with that of the fluid beneath it.

The pressures p_0 and p_1 can be related by applying the Bernoulli equation along the dividing streamline. If p_s denotes the pressure at the stagnation point, which, as will be shown in § 5, must be located some distance h_s below the upper boundary, then

$$p_0 + \tfrac{1}{2}\rho c^2 = p_s - \rho g h_s. \tag{4}$$

Surface tension will cause the pressure inside the air cavity to exceed the pressure on the liquid side of the interface so that

$$p_1 = p_s + \frac{\sigma}{r}, \tag{5}$$

where σ is the surface tension and r is the radius of curvature of the air–water interface at the stagnation point. Combining (4) and (5) gives

$$p_1 = p_0 + \tfrac{1}{2}\rho c^2 + \rho g h_s + \frac{\sigma}{r}. \tag{6}$$

The pressure differential $p_1 - p_0$ may now be eliminated from (2) and (3) and, if these equations are normalized by dividing respectively by $\frac{1}{2}\rho g h_0^2$ and $\frac{1}{2}\rho g c h_0^2$, the following equations result:

$$F^2 + 1 = \frac{2F^2}{H_1} + H_1^2 + \frac{\Sigma}{2R} + 2H_s, \tag{7}$$

$$2 = \frac{F^2}{H_1^2} + 2H_1 + \frac{\Sigma}{2R} + 2H_s, \tag{8}$$

Here $F = c(gh_0)^{-\frac{1}{2}}$ is the cavity Froude number, $H_1 = h_1/h_0$ is the depth ratio of the frontal region, $R = r/h_0$ is the normalized radius of curvature at the stagnation point, $\Sigma = 4\sigma/\rho g h_0^2$ is a surface-tension parameter as defined by Gardner & Crow (1970), and $H_s = h_s/h_0$ is the normalized stagnation-point displacement.

Equations (7) and (8) differ from those derived by Gardner & Crow (1970) and from Benjamin's original work in that they allow for displacement of the stagnation point away from the upper boundary. Also, the forces due to surface tension at the upper and lower air–water interfaces have been omitted from (7) and (8), and would involve an additional term of order Σ on the right-hand side of each of these equations. In deep ducts, these terms are typically some orders of magnitude less than the included surface-tension effects, which are of order Σ/R and were introduced through the effect of surface tension on the stagnation pressure in (5).

Equations (7) and (8) can readily be solved to give the steady energy-conserving flow

$$F = H_1 = \tfrac{1}{2} - \frac{\Sigma}{4R} - H_s. \tag{9}$$

Thus the interface in ideal fluid flow is located centrally in the duct. In real fluids, the air cavity extends below the duct centre line, and the celerity of the cavity is reduced. Real-fluid effects will not be considered further in this section, which is aimed at quantitative clarification of the dominant forcing due to gravity and the fluid inertia. The cavity in an ideal-fluid experiment would intrude into the duct with celerity $c = \frac{1}{2}(gh_0)^{\frac{1}{2}}$, and since the depths of the cavity and the flow beneath it are the same the velocity of this flow must be equal and opposite to that of the cavity.

Consider now the upstream influence of a weir located at the open end of the duct if it is raised by some small amount. Because the flow approaching the weir is sub-critical, a long wave is generated and propagates away from the weir with celerity $c_w = (gh_1)^{\frac{1}{2}}$ relative to the approaching flow. A stationary observer would see this wave slowed to a lesser celerity c'_w given by

$$c'_w = c_w - c = (\sqrt{\tfrac{1}{2}} - \tfrac{1}{2})\,(gh_0)^{\frac{1}{2}} = 0{\cdot}207(gh_0)^{\frac{1}{2}}. \tag{10}$$

The celerity of the front in a stationary frame is equal to $\frac{1}{2}(gh_0)^{\frac{1}{2}}$, which exceeds the wave celerity, and therefore the front remains unaware of the existence of the weir. Evidence of this process was seen in figure 1, where the distance between the cavity front and the bore increased with time.

As the height of the weir is increased further, the long wave steepens to form an undular bore, and eventually a breaking bore. Increasing the height of the weir also increases the celerity of the bore, so that ultimately it can be made to move with the same speed as the cavity front. At this stage there is a dramatic change in the form of the cavity to that shown in figure 3.

An observer travelling with the bore sees the flow in his immediate vicinity as steady. The nature of the bore was determined by the ratio of depths to either side of it, that is the ratio h_2/h_1. When h_2/h_1 was between unity and approximately 1·35, the bore was undular, and was followed by a growing train of waves. For values of h_2/h_1 greater than 1·35, the bore was found to be of the dissipative type and was characterized by a breaking turbulent front, downstream of which the flow was relatively uniform.

Following Whitham (1962), conservation equations for mass, flow force and energy at sections 1 and 2 on either side of the bore are given by

$$\rho u_1' h_1 = \rho u_2' h_2, \tag{11}$$

$$\rho u_1'^2 h + \tfrac{1}{2}\rho g h_1^2 = \rho u_2'^2 h_2 + \tfrac{1}{2}\rho g h_2^2 + [E(2n-\tfrac{1}{2})], \tag{12}$$

$$\tfrac{1}{2}\rho h_1 u_1'^3 + \rho g h_1^2 u_1' = \tfrac{1}{2}\rho u_2'^3 h_2 + \rho g h_2^2 u_2' + [u_2' E(2n-\tfrac{1}{2}) + E(u_2' - c_g)]. \tag{13}$$

Here $E = \frac{1}{2}\rho g a^2$ is the mean energy of the waves per unit surface area (a is the wave amplitude), and n is the ratio of the group velocity c_g to the wave celerity c_w. The primes denote velocities measured from a frame of reference that moves with the bore. The bracketed term in (12) is the radiation stress and in (13) the bracketed term is the work done by the radiation stress on the mean flow plus the radiation of wave energy away from the bore. Since the waves are stationary relative to the bore, it follows that their celerity must be equal in magnitude and opposite in sign to that of the flow and therefore

$$|u_2'| = c_w = \left(\frac{g}{k}\tanh kh_2\right)^{\frac{1}{2}}, \tag{14}$$

where k is the wavenumber.

If the bore is of the undular type then there are four unknowns, u_2', h_2, a and k (both n and c_g are functions of u_2' and kh_2) and (11)–(14) are required for a solution. If the bore is of the dissipative type, there are only two unknowns, u_2' and h_2, and (11) and (12) are sufficient after omission of the bracketed wave term in (12). Solution of these equations leads to the familiar relationship for a hydraulic jump

$$\frac{u_1'^2}{gh_1} = \frac{h_2}{2h_1}\left(\frac{h_2}{h_1}+1\right). \tag{15}$$

Upstream of the bore $h_1 = \frac{1}{2}h_0$, therefore

$$\frac{u_1'^2}{gh_1} = H_2(2H_2+1), \tag{16}$$

where $H_2 = h_2/h_0$.

An explicit relationship for the same variables cannot be obtained for an undular bore; however, calculations by Wilkinson & Banner (1977) showed that, for a given depth ratio h_2/h_1, the parameter u'^2/gh for an undular bore differed from that given by (15) by an amount of the order of $(ak)^2$. Their experiments showed that the maximum value of $(ak)^2$ was 0·04, and this was achieved at incipient breaking when h_2/h_1 was equal to 1·35. Thus $(ak)^2$ is sufficiently small for (15) to be a reasonable approximation for both undular and breaking bores.

Having obtained relationships between the variables in two frames of reference, one moving with the front of the cavity and the other moving with the bore, it remains to close the system by coupling the two frames. Relative to a stationary observer, continuity requires that the velocity at section 1 in figure 4 beneath an energy-conserving cavity be c. If the bore relative to a stationary observer moves with velocity c_b then relative to the bore, the approaching flow has a velocity

$$u_1' = c - c_b = \tfrac{1}{2}(gh_0)^{\frac{1}{2}} - c_b. \tag{17}$$

Elimination of u_1' between (15) and (16) enables the bore Froude number $F_b = c_b(gh_0)^{-\frac{1}{2}}$ to be expressed as a function of the independent variable H_2, whose

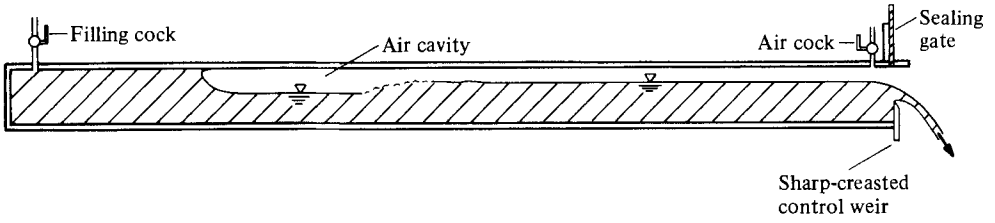

FIGURE 5. Schematic diagram of the experimental facility.

value can be set by suitable manipulation of the weir. Thus the celerity of the bore is governed by the relationship

$$F_b = \tfrac{1}{2} - (\tfrac{1}{2}H_2(2H_2 + 1))^{\frac{1}{2}}. \tag{18}$$

It can be shown from (18) that the bore moves slower than the front if $H_2 < 0{\cdot}781$. Thus the steady flow shown in figure 3 can only occur when $0{\cdot}781 < H_2 < 1$. In this range Benjamin's original analysis holds and the celerity of the front is determined by the conservation relationship (7) for flow force. For values of H_2 between $\frac{1}{2}$ and 0·781 the flow as a whole is unsteady, with the front behaving as an energy-conserving flow followed by a slower-moving bore whose celerity is determined by the downstream control through (18).

4. Experiments

The experiments were directed towards clarifying the various flow regimes and were performed in a Perspex-walled duct, 3 m in length and having an internal width of 100 mm and a height of 100 mm. One end of the duct was sealed, and at the other end a sliding gate was installed, which when in place sealed the duct completely. Throttling was provided by a sharp-crested weir located adjacent to, and immediately downstream from, the sliding gate. Figure 5 shows the layout of the experimental facility.

The depth ratio H_2 could be adjusted to any desired value between 0·5, when the sharp-edged weir was flush with the bottom of the duct, thus generating no upstream influence, and 1, when the weir extended the full height of the duct.

A second series of experiments, aimed primarily at clarifying the effect of surface tension on the motion of the front, was performed in a deeper duct, also 3 m in length but with cross-sectional dimensions of 200 by 400 mm. In one group of tests the 200 mm side was uppermost while in another group the 400 mm side was uppermost.

The duct was inclined slightly while it was filled with water so that the air could escape through a small vent above the weir. This vent was closed and the duct, completely filled with water, was returned to the horizontal position prior to removing the sealing gate and thus starting the experiment. The discharge from the duct was controlled by the crest level of the sharp-crested weir.

The advance of the air cavity along the duct was photographed at 0·5 s intervals using a 35 mm Nikon camera with motor drive. The exposure time was $\frac{1}{250}$ s. A rotating disc timer adjacent to the duct enabled the time at which each photograph was taken to be determined to better than $\frac{1}{100}$ s. Markers at 20 cm intervals along the roof of the duct (see figure 1) enabled the velocity of the cavity to be determined at ten or more sections along the tank to an accuracy of better than $\pm 2\,\%$.

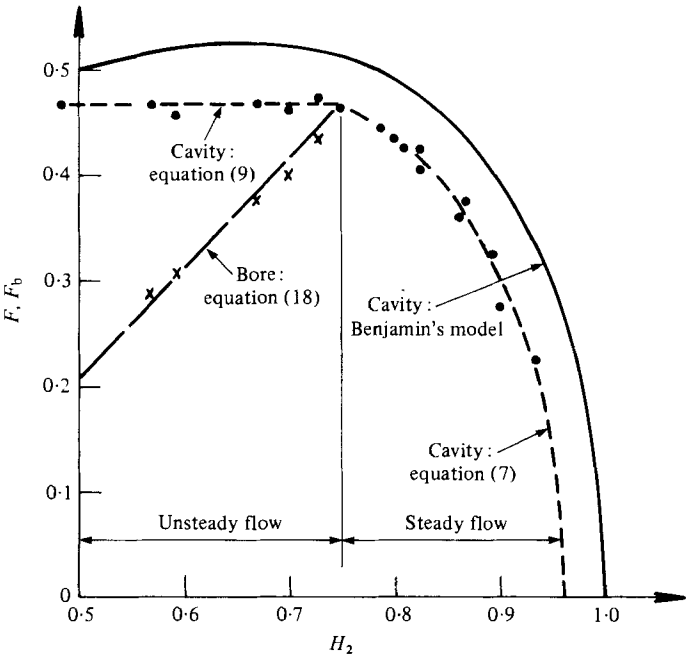

FIGURE 6. Cavity Froude number (●) and normalized celerity of the bore (×) as functions of the downstream depth ratio. $\Sigma = 3 \times 10^{-3}$ for all data shown.

In accordance with Daly & Pracht (1968), who investigated numerically the behaviour of gravity-current surges produced by the removal of a barrier separating fluids of slightly differing densities, the celerity of the air cavity was found to achieve a constant value within a distance comparable to the height of the duct. No systematic variation of the cavity celerity was detectable beyond this point.

Experimental values of the normalized celerities of the cavity and the bore (F and F_b respectively) are plotted against the far-downstream depth H_2 in figure 6. The continuous curve shows the relationship as originally calculated by Benjamin for the motion of the cavity front, and corresponds to (7) with $H_s = 0$ and $\Sigma/R = 0$. The dashed curves between $0{\cdot}5 < H_2 < 0{\cdot}75$ correspond to (9) and (18) for the cavity, and the bore respectively, after appropriate values have been substituted for H_s and Σ/R as described in §5. In this range of H_2, the motion of the cavity front is unaffected by throttling of the discharge by the weir.

For $0{\cdot}75 < H_2 < 0{\cdot}96$ the flow is steady and the weir exerts a controlling influence on the motion of the cavity. The dashed curve is a plot of the governing relationship (7) for steady flow, after insertion of appropriate values of H_s and Σ/R. No region of uniform flow corresponding to that denoted by H_1 in figure 4 exists when the flow is steady, and H_1 in (7) should be replaced by H_2.

5. The effects of surface tension and viscosity

Gardner & Crow (1970) clearly demonstrated that surface tension reduced the celerity of air cavities intruding into horizontal ducts. They also found that the shape of the cavity was affected by surface tension.

Surface tension causes the pressure in the cavity interior to exceed the stagnation pressure originally proposed by Benjamin (1968). The end result is a reduction in the celerity of the cavity, as shown in (9). The value of the cavity Froude number is dependent on the radius-of-curvature parameter R and the normalized displacement H_s of the stagnation point. However, neither of these parameters can be controlled independently, and further relationships must be sought in order to determine their magnitudes.

Gardner & Crow assumed the stagnation point to be located on the upper boundary, $H_s = 0$. They argued, that because velocities in the vicinity of the stagnation point are very small, the radius of curvature there should be independent of the cavity celerity and therefore equal to the value for a blocked condition, where surface tension exactly balances the hydrostatic forces and the cavity is stationary in the duct. While their experimental data indirectly support this assumption in small ducts ($\Sigma > 10^{-2}$), the flow in the vicinity of the leading edge of the cavity is more complex than was proposed in their model.

As the cavity progresses along the duct, the no-slip condition at the rigid boundaries, combined with surface tension, causes a film of water to remain attached to the roof. Therefore, relative to the cavity, the flow divides, with the bulk of the flow passing beneath the cavity, but with a small fraction flowing above the cavity to form the film. It follows that the dividing streamline, and therefore the stagnation point, must be located below the roof of the duct. Furthermore, because the velocity in the vicinity of the stagnation point is low, while the velocities above the dividing streamline far upstream and far downstream of the stagnation point are equal to c, continuity dictates that the depression of the stagnation point will be many times the film thickness.

When an air cavity intrudes into a duct containing water that is initially at rest, the only motions are those that are induced by the cavity itself. The induced motions decrease rapidly with distance ahead of the cavity and it can be shown that the boundary-layer thickness at the roof of the duct is appreciably less than the distance between the stagnation point and the roof.

Hence the general features of the flow in the immediate vicinity of the stagnation point (and only in this region) can be obtained from an inviscid model consisting of a source located at (0, 1), its mirror image at (0, -1) and a uniform flow with velocity V given by $\psi = Vy$. The resulting stream function is

$$\psi = Vy + \arctan\frac{y-1}{x} + \arctan\frac{y+1}{x}. \tag{19}$$

The flow pattern described by this stream function depends on the value assigned to V. When $V \leqslant 1$ a single half-body results, exhibiting symmetry about the x-axis; however, this flow is not relevant to the present study. When $V > 1$ two half-bodies result, placed symmetrically about the x-axis; the flow in the lower domain is shown in figure 7. The x-axis represents the roof of the duct, and it can be seen that the flow divides at a point above the nose of the cavity. One stream passes above the cavity to form the film attached to the roof, while the bulk of the flow passes beneath the cavity. Increasing the value of V has the effect of reducing the ratio of the nose height to the depth of the flow above the cavity, that is the ratio of nose height to the film thickness. The value of V selected as being appropriate to the model was that which gave the same ratio of nose height to film thickness as was observed in experiments.

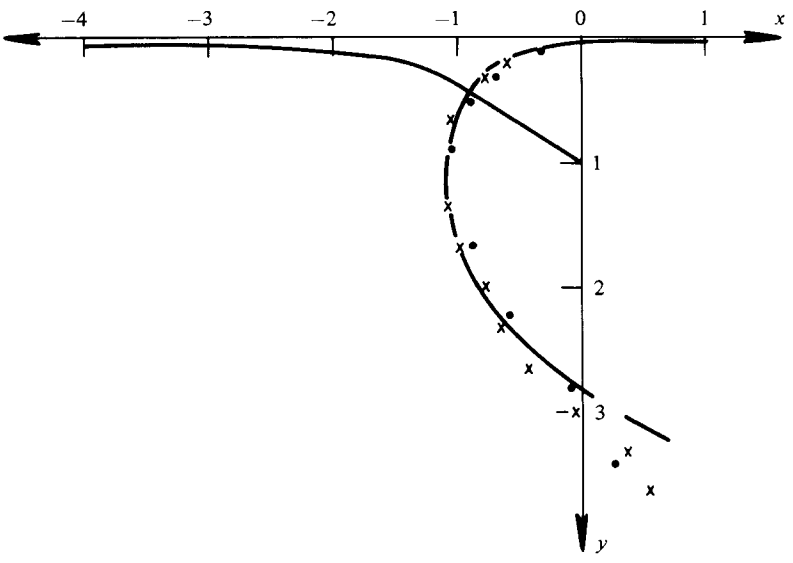

FIGURE 7. The form of the dividing streamline in the potential-flow model. Matching the ratio of film thickness to leading-edge displacement from the boundary set $\psi_0 = 0{\cdot}0333$ for $\Sigma = 3 \times 10^{-3}$. Observed cavity profiles are shown for $F = 0{\cdot}46$ (×) and $F = 0{\cdot}33$ (●).

The thickness of the film remaining on the roof of the duct was found by wiping a measured area of the roof with a sponge immediately after the passage of the air cavity and then weighing the sponge to determine its increased mass. The film thickness was found to be $0{\cdot}1 \pm 0{\cdot}04$ mm for an energy-conserving flow in the 100 mm deep duct. The distance between the nose of the cavity and the boundary was measured directly from photographic enlargements and the mean value was found to be $3{\cdot}3 \pm 0{\cdot}5$ mm. The ratio of these two dimensions gave $V = 1{\cdot}11$ and the ψ-value of the dividing streamline $\psi_0 = 0{\cdot}0333$.

Figure 7 gives a comparison between the observed profile of the cavity and that described by the stream function (19); and agreement between the two in the frontal region is surprisingly close. However, the validity of an inviscid model to predict flow patterns, in particular the location of the stagnation point, so close to a solid boundary, must be examined.

The potential model gives the velocity distribution along the upper boundary as

$$u_{y=0} = V + \frac{x}{x^2+1}. \tag{20}$$

The boundary itself, viewed from the same frame of reference, moves with velocity V; and because $x < 0$ in the area of interest the boundary moves faster than the adjacent fluid, with the velocity difference across the boundary layer u_δ given by

$$|u_\delta| = \frac{x}{x^2+1}, \tag{21}$$

which asymptotes to

$$|u_\delta| = \frac{1}{x} \tag{22}$$

with increasing distance from the cavity.

Thus, far from the cavity the boundary-layer growth would be similar to that produced by a sink at $x = 0$ on a plane stationary boundary coinciding with the x-axis. Such a flow has been investigated by Batchelor (1967), who showed that the depth δ of the vorticity-containing region was given by

$$\delta = \left(\frac{r\mu}{\rho u_\delta}\right)^{\frac{1}{2}}, \tag{23}$$

where for this problem $r = |x|$ and μ is the fluid viscosity. Thus, as one approaches the cavity the increasing velocity difference between the free stream and the boundary produces a convective thinning of the boundary layer which dominates the diffusion of vorticity by viscosity. Substitution of the appropriate values into (23) at a distance of one nose height from the front of the cavity (3·3 mm in the 100 mm duct) gives $\delta = 0{\cdot}1$ mm. Thus the boundary-layer thickness is much less than the height of the nose and the use of an inviscid model to predict the geometry of the dividing streamline is justified.

Having established the location of the stagnation point the validity of equation (9) for the cavity Froude number of the energy-conserving flow can be examined. This flow in the 100 mm duct gave $F = 0{\cdot}46 \pm 0{\cdot}007$, $\Sigma = 3 \times 10^{-3}$, $R = 0{\cdot}033 \pm 0{\cdot}005$ and $H_s = 0{\cdot}015 \pm 0{\cdot}005$. Substitution of these values into (9) yields

$$\begin{aligned} F + \frac{\Sigma}{4R} + H_s &= 0{\cdot}464 + 0{\cdot}023 + 0{\cdot}015 \\ &= 0{\cdot}502 \pm 0{\cdot}017, \end{aligned}$$

in agreement with the value of $\frac{1}{2}$ predicted by the theory. It will be noted that the effect of stagnation-point displacement is comparable with that due to surface tension.

Experiments conducted with lower values of F and constant Σ, and other experiments in which Σ was varied while F remained constant, revealed that the shape and actual dimensions of the cavity in the *immediate vicinity* of the stagnation point remained unchanged. This observation is in accord with the Gardner & Crow assumption, and implies that gravity and surface tension are the dominating influences in that area. It therefore follows that the dimensional groups $\sigma/\rho g r^2$ and h_s/r are constants. Experimental data gave the magnitude of these parameters as $0{\cdot}67 \pm 0{\cdot}25$ and 0·45 respectively. The large relative error in $\sigma/\rho g r^2$ resulted from difficulties in estimating r from the photographs, and could only be accomplished with a consistency of $\pm 20\,\%$. No systematic variation of $\sigma/\rho g r^2$ or h_s/r with F or Σ was noted.

When the above values for $\sigma/\rho g r^2$ and h_s/r are substituted into (9) for the energy-conserving cavity the following relationship results:

$$F = \tfrac{1}{2} - 0{\cdot}68\Sigma^{\frac{1}{2}}. \tag{24}$$

Equation (24) is plotted in figure 8, and is in satisfactory agreement with the data from Gardner & Crow's experiments as well as the present experiments. It should be noted that within the range $10^{-4} < \Sigma < 10^{-1}$ (24) and the equivalent relationship obtained by Gardner & Crow (with their empirical constant $k = 0{\cdot}8$) agree to better than 5 %. The only difference between the two calculations is that the present analysis makes allowance for the departure of the stagnation point from the upper boundary.

Experiments conducted in deeper ducts with correspondingly reduced values of Σ

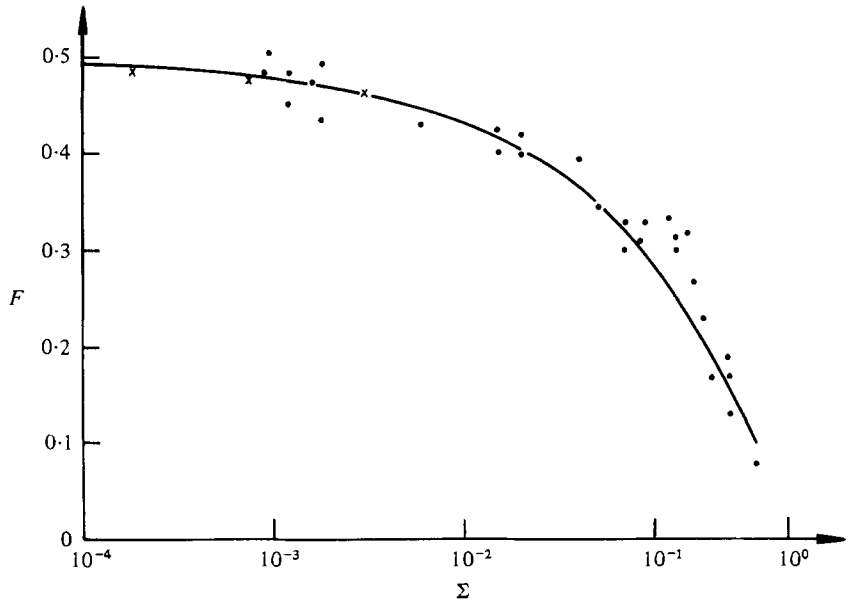

FIGURE 8. Cavity Froude number in energy-conserving flows as a function of the surface tension parameter. ×, present experiments; ●, Gardner & Crow (1970); ——, equation (24).

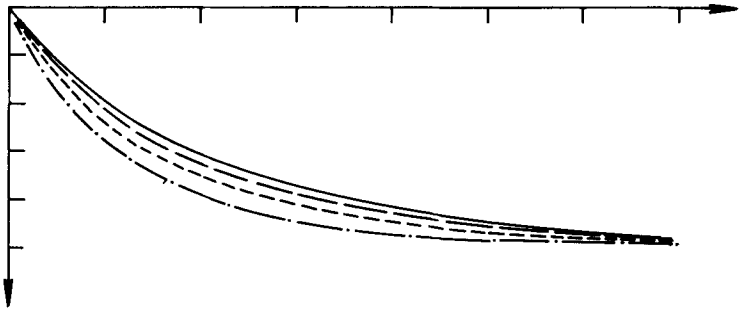

FIGURE 9. Profiles of the energy-conserving cavities for different values of the surface tension parameter. The recumbent leading edges of the cavities have been omitted for clarity. Benjamin's (1968) theoretical profile: ——, $\Sigma = 0$; — —, 2×10^{-4}; - - - - -, 8×10^{-4}; —·—·—, 3×10^{-3}.

confirmed that the surface tension became increasingly less important, and the shape of the cavity approached that of the idealized model originally proposed by Benjamin. This trend is plainly shown in figure 9.

The steady flows are governed by the continuity and flow-force relationships which combined to yield (7), where H_1 now becomes H_2. Substitutions can be made for R and H_s using the previously determined values of $\sigma/\rho g r^2$ and h_s/r. The resulting form of (7) is shown as the dashed curve in figure 6 between $0{\cdot}75 < H_2 < 0{\cdot}96$, and compares favourably with the experimental data. It will be noted that there is a substantial departure from Benjamin's ideal-fluid model (shown by the continuous curve) as H_2 approaches unity.

It could be argued that the reduction of F with increasing values of the surface-tension parameter Σ is due to an accompanying reduction in the Reynolds number. Zukoski (1966) performed an extensive series of experiments in which he studied the

effect of surface tension and viscosity on the motion of long air bubbles in tubes. He found that, provided the Reynolds number defined as $Re = \rho(gh_0^3)^{\frac{1}{2}}/\mu$ is greater than 200, viscosity had no discernible effect on the celerity of the cavity. The Reynolds numbers of the experiments described here were of order 10^5.

A single experiment in which a viscous water–glycerol solution was used with $Re = 2700$ and $\Sigma = 2{\cdot}8 \times 10^{-3}$ gave an initial value of $F = 0{\cdot}451$ that was not significantly different from that obtained with water, where $Re = 8{\cdot}8 \times 10^4, \Sigma = 3{\cdot}0 \times 10^{-3}$ and F was found to be $0{\cdot}464 \pm 0{\cdot}007$. However, the increased boundary friction caused the cavity speed to decrease appreciably as it progressed along the duct, and at no point could the flow beneath the cavity be regarded as uniform.

6. Conclusions

It has been demonstrated that the flow associated with the intrusion of an air cavity into a long horizontal duct may be steady or unsteady, depending on how the flow leaving the duct is controlled. Only when the water depth beneath the cavity is exactly one-half or is greater than about 0·78 of the duct height is steady flow possible. Such flows are described adequately by Benjamin (1968), after allowance has been made for the effects of surface tension.

When the water depth behind the cavity is between 0·50 and 0·78 of the duct height, the cavity can be divided into two distinct regions of uniform parallel flow separated by a bore. The frontal region corresponds to Benjamin's energy-conserving flow where the air–water interface is located at the mid-height of the duct. The frontal region terminates at a bore which travels more slowly than the cavity front and causes a lengthening of the frontal region as it progresses along the duct. The bore can be undular or breaking, depending on the extent of throttling of the flow as it leaves the duct. A second region of uniform parallel flow is observed behind the bore.

Surface tension combined with the no-slip condition at the upper boundary can markedly affect the shape and celerity of the cavity. This becomes more pronounced when the depth of the cavity is small.

The author would like to thank Professor Ian Wood for his helpful comments on a draft of this paper.

REFERENCES

BATCHELOR, G. K. 1967 *An Introduction to Fluid Dynamics.* Cambridge University Press.

BENJAMIN, T. B. 1968 Gravity currents and related phenomena. *J. Fluid Mech.* **31**, 209–248.

DALY, B. J. & PRACHT, W. E. 1968 Numerical study of density-current surges. *Phys. Fluids* **11**, 15–30.

GARDNER, G. C. & CROW, I. G. 1970 The motion of large bubbles in horizontal channels. *J. Fluid Mech.* **43**, 247–255.

SIMPSON, J. E. 1972 Effects of the lower boundary on the head of a gravity current. *J. Fluid Mech.* **53**, 759–768.

WHITHAM, G. B. 1962 Mass, momentum and energy flux in water waves. *J. Fluid Mech.* **25**, 135–147.

WILKINSON, D. L. & BANNER, M. L. 1977 Undular bores. In *Proc. 6th Australasian Hyd. and Fluid Mech. Conf.*, pp. 369–373.

ZUKOSKI, E. E. 1966 Influence of viscosity, surface tension, and inclination angle on motion of long bubbles in closed tubes. *J. Fluid Mech.* **25**, 821–840.